The 7th International Conference of Asian Concrete Federation
"SUSTAINABLE CONCRETE FOR NOW AND THE FUTURE"
30 Oct – 02 Nov, 2016, Hanoi, Vietnam
www.acf2016.vn

EVALUATION OF SIZE EFFECT IN BENDING CHARACTERISTICS OF DFRCC BASED ON BRIDGING LAW

Y. Ozu[1], K. Watanabe[1], A. Yasojima[2], and T. Kanakubo[3]

[1] *Master Program, Dept. of Engineering Mechanics and Energy, University of Tsukuba, Tsukuba, Japan*
[2] *Associate Professor, Dept. of Engineering Mechanics and Energy, University of Tsukuba, Tsukuba, Japan*
[3] *Professor, Dept. of Engineering Mechanics and Energy, University of Tsukuba, Tsukuba, Japan*

ABSTRACT: The purpose of this study is to evaluate the size effect in bending characteristics of ductile fiber-reinforced cementitious composites (DFRCC) with PVA fibers using the bridging law considering fiber orientation. Four-point bending test with experimental factor of specimen size was conducted. From the test results, the size effect that bending strength decreases with increasing of the specimen size was recognized. The bridging law considering fiber orientation was calculated based on the previous study, and the section analysis using the bridging law was performed. From the analysis results, the size effect can be evaluated by the bridging law which shows the tendency that the axial orientation of the fibers becomes stronger with decreasing of specimen size.

1 INTRODUCTION

Ductile fiber-reinforced cementitious composites (DFRCC), in which short fibers with a certain percentage of volume fraction are mixing in mortar or concrete, show the improved tensile and bending characteristics of cementitious composites. DFRCC is applied to the structural elements expecting high performance in ductility and tensile characteristic, because short fibers bridge the crack after first cracking and transfer the tensile force. Some previous studies indicated that the tensile characteristics of DFRCC is strongly affected by fiber orientation and distribution in matrix (e.g. Laranjeira et al. (2012)). However, there is little study evaluating the effect of fiber orientation to tensile characteristics of DFRCC quantitatively.

The tensile performance of DFRCC is characterized by the bridging law (tensile stress – crack width relationship). The bridging law can be expressed by the sum of the pullout properties of single fiber. The mechanical characteristics of DFRCC can be evaluated accurately using the bridging law considering fiber orientation. On the other hand, structural elements using DFRCC show the size effect that the strength decreases with increasing of cross-sectional size (Kanakubo et al. (2007)). Moreover, it is considered that the size effect is also caused by two-dimensional fiber orientation. The strength and the ductility increase for small size specimens due to two-dimensional fiber orientation along the wall of the mold.

In this study, the four-point bending tests for different sizes of specimens using DFRCC with PVA fibers are conducted. The size effect observed in the experiment is evaluated quantitatively using the bridging

law considering fiber orientation.

2 CALCULATION OF BRIDGING LAW CONSIDERING FIBER ORIENTATION

Bridging law can be expressed by the sum of the pullout behavior of each single fiber bridging crack plane considering bond properties between single fiber and matrix, including the snubbing effect and the fiber strength degradation. The snubbing effect shows the increment of the pullout load due to the edge reaction when fiber is embedded to matrix with inclined angle. The fiber strength degradation expresses the decrement of fiber strength because the surface of fiber is roughed by the asperity of the matrix when fiber has inclined angle. The fiber orientation in the crack plane is evaluated by probability density function (PDF) which expresses the distribution of orientation angle of the fibers that bridge the crack (Kanakubo et al. (2016)). Figure 1 shows the definition of coordinate system and orientation angle of fiber.

2.1 Pullout property of single fiber

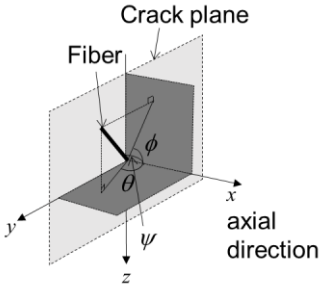

Figure 1. Definition of orientation angle.

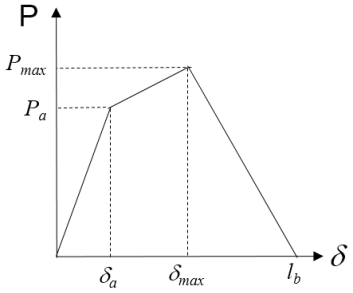

Figure 2. Pullout model of single fiber.

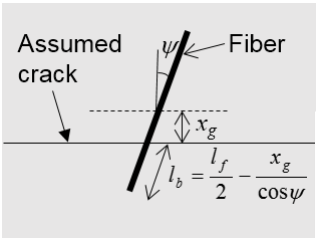

Figure 3. Definition of embedded length.

Table 1. Parameter for the pullout model of single fiber

Parameter	Used value
First peak load P_a (N)	1.5
Crack width at P_a (mm)	0.2
Maximum load P_{max} (N)	3.0
Crack width at P_{max} (mm)	0.45
Snubbing coefficient f	0.5
Fiber strength σ_{fu} (MPa)	569
Fiber strength reduction factor f'	0.3
Fiber diameter d_f (mm)	0.10
Fiber length l_f (mm)	12

The pullout tests of single fiber have been conducted by several researchers to evaluate the bond properties of fiber. Figure 2 shows the model of the relationship between the pullout load and the pullout displacement of single fiber used in current study. Table1 shows the value of each parameter for the pullout model of single fiber. The relationship is modeled by tri-linear model considering chemical bond and friction between PVA fiber and matrix (Redon et al. (2001)). The first peak load P_a corresponds to the debonding of the chemical bond and pullout load increases to the maximum load P_{max}. After P_{max}, single fiber is pulled out completely when the pullout displacement becomes equal to the embedded length l_b. Figure 3 shows the definition of the embedded length l_b that is calculated by orientation angle ψ in Figure 1 and the distance between the midpoint of fiber and assumed crack surface. The first peak load, the maximum load, and each pullout displacement are determined based on the previous study (Kanakubo et al. (2016)). The values of snubbing coefficient, fiber strength, and fiber strength reduction factor are assumed to be 0.5, 569MPa, 0.3, respectively (Kanda and Li (1999), Asano (2014)).

2.2 *Fiber orientation distribution*

The elliptic function has been introduced as the PDF in order to evaluate the fiber orientation distribution quantitively in the previous study (Kanakubo et al. (2016)). Figure 4 shows the example of relative frequency distribution by the visualization simulation of PVA fibers in the matrix using a sodium silicate solution (water glass) which is clear and colorless, and has high viscosity such as the matrix of DFRCC (Miyaguchi et al. (2014)). The solid line in Figure 4 shows the elliptic distribution. The elliptic distribution is expressed by the orientation intensity k and the principal orientation angle θ_r. The relative frequency for each orientation angle of fiber orientation distribution is transformed into plane coordinates (x^*-y^*) with the argument to be equal to orientation angle. The relative frequency in x*-y* coordinates are approximated by the ellipse function using the least square method. The ratio of the radii of the approximated ellipse (a/b) is defined as orientation intensity, k, and the angle between the radius a and the axis x^* is defined as principal angle, θ_r. The range of the value of the principal angle θ_r is -45° to +45°. The tendency of fiber orientation toward the direction of the principal angle is expressed by the value of k. When the fibers tend to orient to θ_r, the value of k becomes larger than 1, and when they orient to the perpendicular direction to θ_r, the value of k becomes smaller than 1. The random orientation is shown as the value of k = 1.

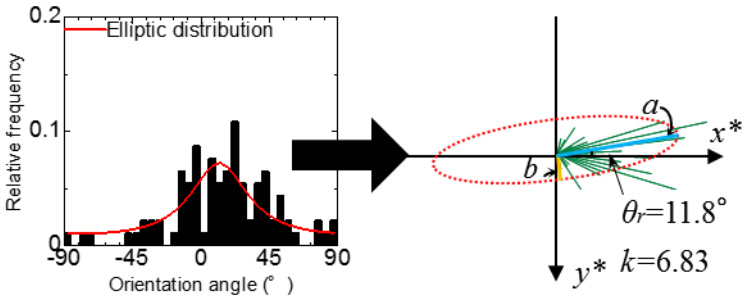

Figure 4. Elliptic distribution for fiber orientation.

2.3 *Calculation of bridging law*

The bridging law considering fiber orientation is calculated by combining the pullout properties of the single fiber with the elliptic distribution as the PDF which evaluate the fiber orientation quantitatively as given by equation (1).

$$P_{bridge} = \sum_h \sum_j \sum_i P_{ij}(\delta,\psi) \cdot p_{xy}(\theta_i) \cdot p_{zx}(\phi_j) \cdot p_x(y_h, z_h) \cdot \Delta\theta \cdot \Delta\phi \cdot (\Delta y \cdot \Delta z) \quad (1)$$

P_{bridge}	= bridging force
$P_{ij}(\delta,\psi)$	= tensile force of single fiber
$p_{xy}(\theta_i)$, $p_{zx}(\varphi_j)$	= probability based on elliptic distribution for x-y plane and z-x plane
$p_x(y_h,z_h)$	= probability of fiber distribution along x axis (constant)
θ, φ	= refer to Figure 1

Figure 5 presents the example of bridging law calculated considering the fiber orientation. The calculated bridging force is converted to tensile stress dividing the force by cross-sectional area. The parameters for calculation are already shown in Table1, and principal angle θ_r is assumed to be equal to 0° (axial direction) in the calculation. The curves in the figure show the bridging laws for each value of orientation intensity k (k=0.4, 1.0, 4.0). Figure 5 shows the stress only by the bridging law, that means the crack strength of the matrix is not expressed in the figure. As shown in Figure 5, tensile stress remarkably decreases after the maximum load due to the rupture of PVA fibers. After that the degradation of the

slope changes gentle. The calculation result for larger *k*, that expresses the longitudinal orientation of fibers, gives larger strength. That means that the fiber orientation greatly affects the bridging law and the tensile behavior.

The calculated bridging law is modeled by the tri-linear model (Figure 6) in order to apply the bridging law to the section analysis explained after. The model is defined by two characteristic points, namely, the tensile strength, σ_{max}, and the changing point of degradation, σ_2. The corresponding crack width for each point is defined as δ_{max}, and δ_2. The tensile stress becomes to be equal to zero when the crack width reaches the half length of fiber (completely pulled out).

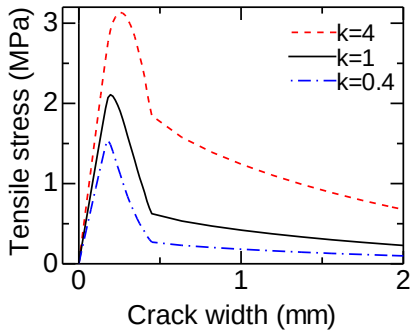

Figure 5. Calculation results of bridging law.

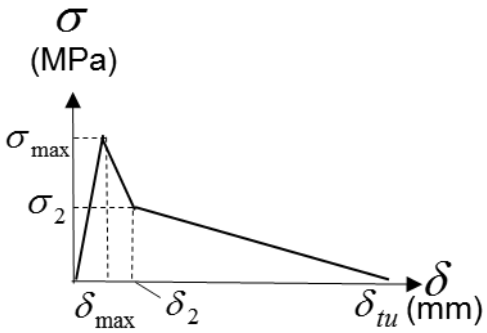

Figure 6. Modeling of bridging law.

3 OUTLINE OF BENDING TEST

3.1 Materials

Table 2 shows mechanical property of PVA fiber and mix proportion of DFRCC applied in this study. The volume fraction of PVA fiber is 2.0%. A total of seven mixing batch was conducted by the same mix proportion.

3.2 Specimens

The dimensions of specimens are shown in Figure 7. The main experimental parameter is the cross-sectional size. Specimens have square or rectangular cross-section. Three series of specimens, (a) small specimen (40x40x160mm), (b) middle specimen (100x100x400mm), and (c) large specimen (180x280x1680mm) were tested. Three small and middle specimens are manufactured by each mixing batch. The number of large specimen is one. Table 3 shows the compression test results of cylinder (φ100-200mm) test pieces and fresh properties.

Table 2. Mechanical properties of PVA fiber

Length of fiber (mm)	Diameter of fiber (mm)	Tensile strength (MPa)	Elastic modulus (GPa)
12	0.10	1200	28

Table 3. Fresh properties and compression test results

Temperature (°C)	Air content (%)	Compressive strength (MPa)	Elastic modulus (GPa)
24.5	1.8	45.6	13.9

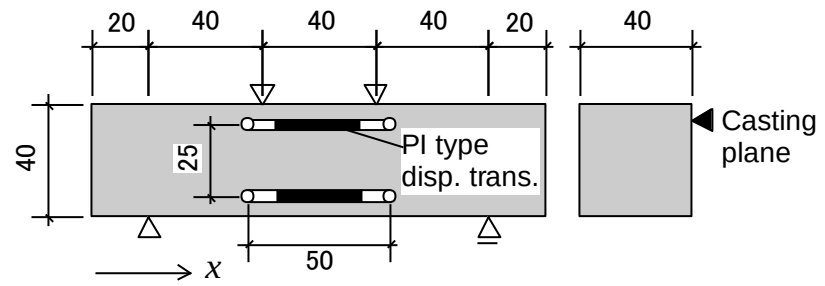

(a) Small specimen.

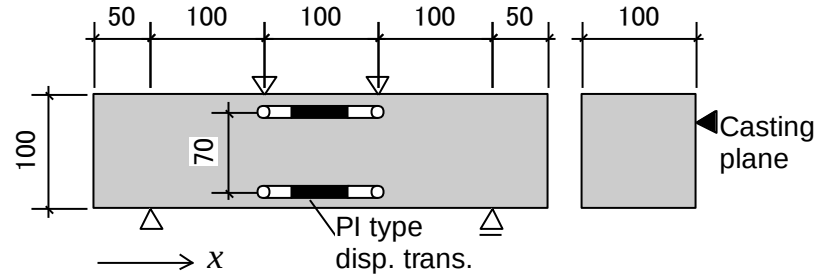

(b) Middle specimen.

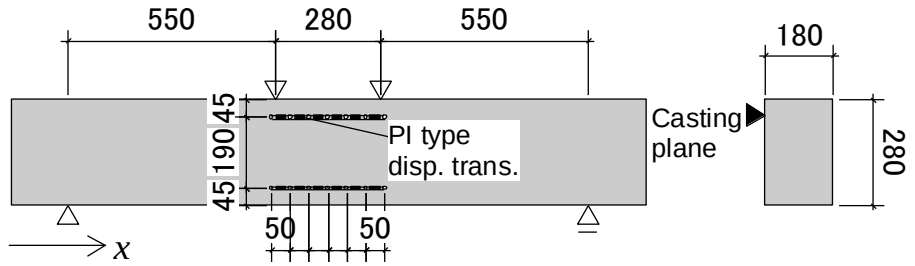

(c) Large specimen.

Figure 7. Dimensions of specimens.

3.3 Method of loading and measurements

Four-point bending tests were carried out using a universal testing machine of 500kN capacity for small and middle specimens, and using a universal testing machine of 2000kN capacity for the large specimen. The measurement items for all specimens were load and axial deformation to calculate average curvature of pure bending region. In addition, six pi type displacement transducers of gauge length of 50mm were set along the upper and lower position in the case of the large specimen.

4 TEST RESULTS

The examples of the specimens after loading are shown in Figure 8. The loading points are indicated by arrows. In the small specimens, there was only one crack within pure bending region, and the crack was gradually opened, after that, specimens fractured. On the other hand, in the middle specimens and the large specimen, there were one or two cracks within pure bending region, after that, either one of the two cracks was opened and load decreased.

In order to compare the effect of the difference of the specimen size, bending stress, which is bending moment divided by section modulus, and bending strain, which is curvature multiplied by depth of the specimen, are defined. Figure 9 shows the relationships between bending stress and bending strain for each specimen size except the specimens that fractured at the out of pure bending region. As shown in Figure 9, in the case of small specimens, after decreasing the load due to cracking, the load gradually

increased again. After the peak load, the load moderately decreased. In the case of middle and large specimens, the load degradation at cracking was relatively small, the load slightly decreased after peak load. The higher maximum load and the deformability were observed for the specimens in which the two or more cracks took place. The size effect that bending strength decreases with increment of specimen size is recognized.

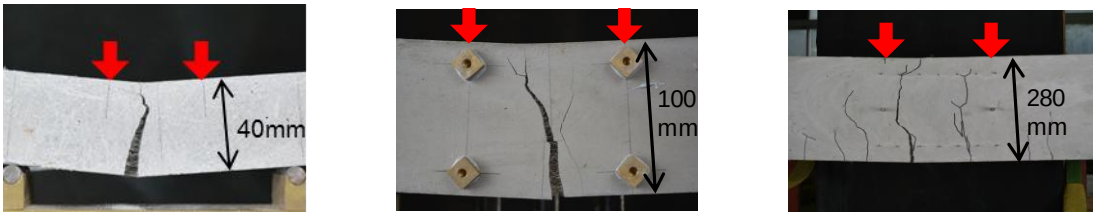

(a) Small specimen. **(b) Middle specimen.** **(c) Large specimen.**

Figure 8. Specimens after loading.

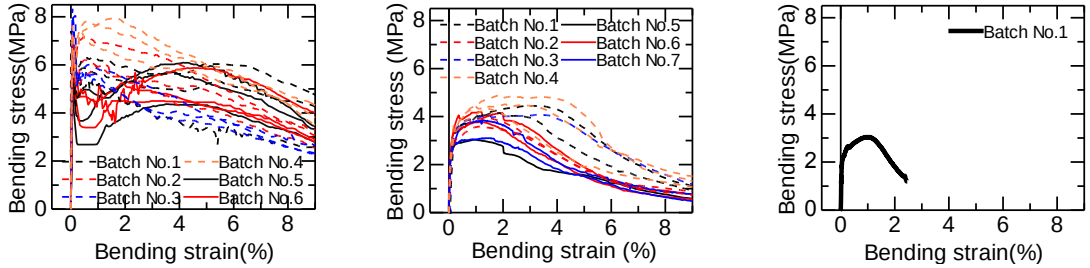

(a) Small specimen. **(b) Middle specimen.** **(c) Large specimen.**

Figure 9. Bending stress - bending strain curve.

5 SECTION ANALYSIS

5.1 Stress – strain model of DFRCC

The section analysis employing the bridging law of DFRCC considering fiber orientation is conducted for each size of specimens, and the analysis results are compared with test results. Figure 10 and Table 4 show the stress-strain model of DFRCC and the values of the parameters of the model, respectively. The compressive stress-strain model is the parabolic model and the compression test results of the test pieces (Table 3) are utilized as the parameters of the model. The tensile stress-strain model is derived from the model of the bridging law (Figure 6).

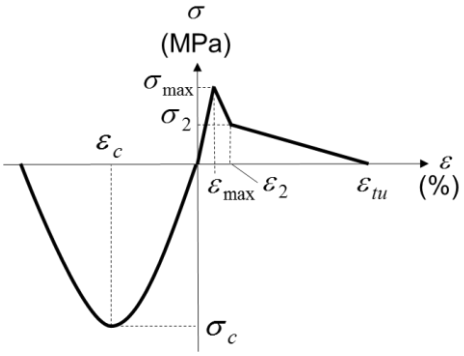

Figure 10. Modeling of stress - strain curve of DFRCC.

Table 4. Parameters of the stress - strain model

Specimen size	Small			Middle			Large		
Orientation intensity k	0.4	1.0	4.0	0.4	1.0	4.0	0.4	1.0	4.0
Compression strength σ_c (MPa)	43.6			43.6			43.6		

Strain at σ_c, ε_c (%)	0.45			0.45			0.45		
Average crack spacing (mm)	40			65.4			140		
Maximum tensile stress σ_{max} (MPa)	1.54	2.11	3.13	1.54	2.11	3.13	1.54	2.11	3.13
Strain at σ_{max}, ε_{max} (%)	0.45	0.49	0.64	0.28	0.30	0.39	0.13	0.14	0.18
Second peak tensile stress σ_2 (MPa)	0.27	0.62	1.85	0.27	0.62	1.85	0.27	0.62	1.85
Strain at σ_2, ε_2 (%)	1.13			0.69			0.32		
Tensile ultimate strain ε_{tu} (%)	15.0			9.18			4.29		

The parameters of the tension model based on the bridging law are determined by orientation intensity *k*. Moreover, the crack width of the bridging law is transformed into the strain dividing by the average value of crack spacing observed in the bending test. The crack spacing is obtained as the length of pure bending region divided by the number of cracks. In this paper, θ_r is assumed to be equal to 0° (axial direction of specimens).

5.2 Analysis results

5.2.1 Analysis for random orientation

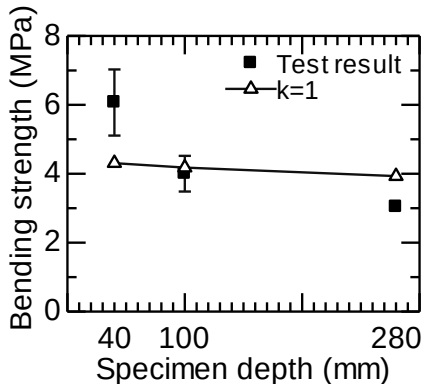

Figure 11. Analysis results (*k*=1).

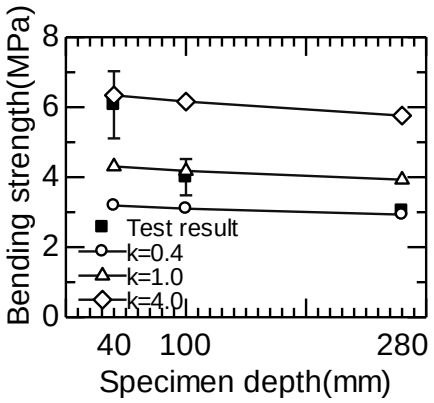

Figure 12. Analysis results (*k*=4, 1, 0.4).

Figure 11 shows the comparison of bending strength between test results and analysis results in the case of random orientation (*k*=1). The bending test results are plotted by square marks with the error bars that exhibit the standard deviations of test results for specimens of each size. The analytical bending strength decreases with increasing specimen size in spite of using the same bridging law (same value of *k*), because the strain gradient in cross-section increases with the increment of the cross-sectional size. As shown in the figure, the test result mostly corresponds to the analysis result only for the middle specimen.

5.2.2 Analysis considering fiber orientation

Orientation intensity *k* for small specimens is generally 4 in the visualization simulation in the previous study (Miyaguchi et al. (2014)). Therefore, the section analysis is carried out again using the different value of *k*. The assumed value for *k* is set to 4 for the small specimen, and set to 0.4 for the large specimen. The *k* value of 4 and 0.4 shows that the fibers tend to orient longitudinally and toward perpendicular to axial direction of a specimen, respectively. The comparison between test results and analysis results is shown in Figure 12. The test results of small specimen, middle specimen, and large specimen show good agreements with analysis results. These results indicate that PVA fibers in small specimens tend to orient along axial direction, and there is a tendency that orient toward perpendicular to axial direction with increasing of specimen size.

From the observation of the flow of the DFRCC pouring in the case of large specimen, the matrix spread concentrically from the position of inflow of DFRCC. This observation suggested that fibers orient concentrically and tend to turn toward perpendicular to axial direction.

6 CONCLUSION

In this study, the size effect in bending characteristics of DFRCC was confirmed experimentally. The bridging law considering fiber orientation is calculated based on the previous study and the tri-linear model of the bridging law is proposed. The size effect in the bending strength can be evaluated by the section analysis using the tensile stress-strain model of DFRCC that shows the tendency of the stronger orientation toward the axial direction with decreasing specimen size.

7 ACKNOWLEDGEMENT

This study was supported by the JSPS KAKENHI Grant Number 26289188.

8 REFERENCES

Asano, K. (2014) “Study on Fiber Orientation and Bridging Constitutive Law in High Performance Fiber Reinforced Cementitious Composites”, *Doctoral thesis of University of Tsukuba*. (in Japanese)

Kanakubo, T., Shimizu, K., and Kanda, T. (2007) “Size Effect on Flexural and Shear Behavior of PVA-ECC”, *Structures under Extreme Loading, Proceedings of Protect 2007*.

Kanakubo, T., Miyaguchi, M., and Asano, K. (2016) “Influence of Fiber Orientation on Bridging Performance of Polyvinyl Alcohol Fiber-Reinforced Cementitious Composite”, *ACI Materials Journal*, Vol.113, No.2: 131-141.

Kanda, T., and Li, V. C. (1999) “Effect of Fiber Strength and Fiber-Matrix Interface on Crack Bridging in Cement Composites”, *ASCE Journal of Engineering Mechanics*, Vol.125, No.3: 290-299.

Laranjeira, F., Aguado, A., Molins, C., Grünewald S., Walraven, J., and Cavalaro, S. (2012) “Framework to predict the orientation of fibers in FRC: A novel philosophy”, *Cement and Concrete Research*, 42: 752-768.

Miyaguchi, M., Tsukizaki, R., Man, Shimei. Asano, K., and Kanakubo, T. (2014) “Study on Fiber Orientation of HPFRCC: Part2: Visualization Experiment of Fiber Orientation”, *Summaries of technical papers of annual meeting of Architectural Institute of Japan,* 181-182. (in Japanese)

Redon, C., Li, V.C., Wu, C., Hoshiro, H., Saito, T., and Ogawa,A. (2001) “Measuring and Modifying Interface Properties of PVA Fibers in ECC Matrix”, *ASCE Journal of Materials in Civil Engineering*, Vol.13, No.6: 399-406.